Indian Journal of Pure & Applied Physics
Vol. 52, December 2014, pp. 799-811

Study of spectroscopic properties, thermodynamic, NBO, quantum chemical calculations and Curie plot of 3′-(triflouromethyl)acetophenone

V Balachandran[a]*, S Lalitha[b] & S Rajeswari[b]

[a]Centre for Research, Department of Physics, A A Government Arts College, Musiri 621 211, India

[b]P.G. & Research Department of Physics, Periyar EVR College (Autonomous), Tiruchirappalli 620 023, India

*E-mail:brsbala@rediffmail.com

Received 21 May 2013; revised 15 January 2014; accepted 17 September 2014

The experimental spectra 3′-(triflouromethyl)acetophenone have been assigned based on DFT calculations at B3LYP level of theory using the standard 6-31+G(d) and 6-311++G(d, p) basis sets and scaling of the calculated frequencies. In fitting the calculated wavenumbers to the experimental ones, two different scaling procedures called "scaling wavenumbers with dual scale factors" and "uniform scaling procedure", were preceded. These procedures have yielded results in very good agreement with the experiment and thus proved the necessity for an efficient scaling procedure over the calculated harmonic wavenumbers for performing a correct vibrational spectroscopic analysis on the basis of B3LYP calculations. The HOMO–LUMO energy gap of the molecule has been calculated and used for predicting the site for electrophilic and nucleophilic attack. The presence of the flouro-methyl group has a strong effect on the physical structure of the compound. The NBO and Mulliken population analysis have been performed on the molecule for understanding the charge distribution, molecular geometry, hybridization and the strength of different bonds forming the molecule. The thermodynamic and paramagnetic susceptibility variations with temperature are recorded for different temperature ranges.

Keywords: 3′-(triflouromethyl)acetophenone, DFT, HOMO–LUMO, NBO, Thermodynamic parameters

1 Introduction

Fluorinated compounds have become very important on account of their wide range applications. Fluoro compounds are widely used as heat transfer fluids, chemical intermediaries, polymers etc.[1] Acetophenone is a raw material for the synthesis of some pharmaceuticals[2,3] and is used to create fragrances that resemble almond, cherry, honeysuckle, jasmine and strawberry. It is used in chewing gum[4]. Being prochiral, acetophenone is also a popular test substrate for asymmetric transfer hydrogenation experiments and is also commonly used as a flavoring agent in many cherry flavored sweets and drinks. Acetophenone occurs naturally in many foods like apple, cheese, apricot, banana, beef and cauliflower. It was marketed as a hypnotic and anti-convulsant under brand name hypnone. It was considered to have superior sedative effects to both paraldehyde and chloral hydrate[5]. This paper deals with the vibrational spectroscopic studies of 3′-(triflouromethyl)acetophenone (3′-TFMA).

2 Experimental Details

The sample in the solid form was purchased from the Lancaster Chemical Company (UK) with a purity of greater than 98% and used as such without purification. The FT-IR spectrum of the compound was recorded in the frequency region 4000-400 cm^{-1} on a NEXUS 670 spectrophotometer equipped with an MCT detector, a KBr pellet technique. The FT-Raman spectrum of title compound has been recorded in the frequency region 3500-100 cm^{-1} on a NEXUS spectrophotometer equipped with Raman module accessory with Nd:YAG laser operating at 1.5 W power continuously with 1064 nm excitation. The spectral measurements were carried out at central Electro Chemical Research Institute (CECRI) Karaikudi, Tamilnadu, India.

3 Computational Details

The molecular geometry optimizations, energy and vibrational frequencies were carried out with the Gaussian 09 software package[6] at the DFT (B3LYP) levels supplemented with the standard using BLYP/6-31+G(d) and BLYP/6-311++G(d,p) basis sets. The Cartesian representation of the theoretical force constants have been computed at optimized geometry by assuming C_1 point group symmetry. The vibrational modes were assigned by means of visual inspection[7] using the GAUSSVIEW program.

As the molecule is non-planar and asymmetrically substituted, vibrations get coupled with contributions from different bond oscillators. It would thus be a difficult problem to make assignments on the basis of 'group-frequencies concept' and spectra alone. Therefore, to aid the assignment, normal coordinate calculations were performed using MOLVIB program[8]. By taking B3LYP/6-311++G(d,p) result as input, we computed normal modes and potential energy distributions (PEDs).

For the plots of simulated IR and Raman spectra, pure Lorentzian band shapes were used with a band width of ±1 cm^{-1}. The prediction of Raman intensities were carried out by the following procedure. The Raman activities (S_i) calculated by the Gaussian 09 program were converted to relative Raman intensities (I_i) using the following relationship derived from the basic theory of scattering[9–11].

$$I_i = \frac{f(\nu_0 - \nu_i)^4 s_i}{\nu_i[1-\exp(-hc\nu_i)/kT]}$$

where ν_0 is the exciting frequency (in cm^{-1}), ν_i is the vibrational wave number of the i^{th} normal mode, h, c, k the universal constants and f is a suitably chosen common normalization factor for all peak intensities.

4 Results and Discussion

4.1 Structural properties

The introduction of triflouromethyl substituent on the acetophenone ring is of great importance in determining its structural and vibrational properties. It is found that replacing hydrogen by bulky flouromethyl group has caused slight perturbation in the ring atoms which are closest to the substituents. It is seen that geometry of the remaining part of the benzene ring is relatively unperturbed. The substituent has insignificant impact on the bond angle of the compound. The bond lengths and bond angles of 3′-TFMA are in good agreement with the derived parameters of the related molecule[12]

4.2 Vibrational frequencies and normal co-ordinate analysis

The labeling of atoms of the title compound is shown in Fig. 1. The most optimized geometrical parameters were also calculated and are presented in Table 1. The detailed vibrational analysis of fundamental modes with FT-IR and FT-Raman experimental frequencies using BLYP/6-31+G(d) and BLYP/6-311++G(d,p) basis sets of the title compound

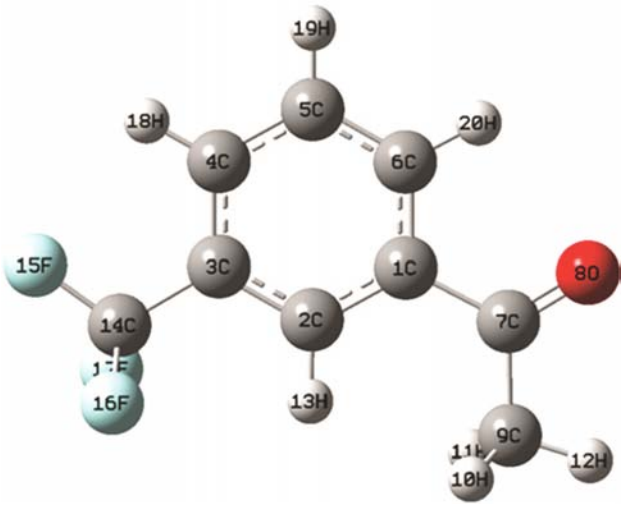

Fig. 1 — Optimized geometrical structure of 3′-(triflouromethyl) acetophenone

are reported in Table 2. The 3′-TFMA has 20 atoms and so it has 54 normal modes of vibration. It belongs to the point group symmetry C_1 with only identity (E) symmetry operation. The observed and computed infrared and Raman spectra of 3′-TFMA are shown in Figs 2 and 3.

4.3 Vibrational assignments

The vibrational analysis of 3′-TFMA is performed on the basis of the characteristic vibrations of carbonyl, flouro, methyl and phenyl ring modes. The computed vibrational wavenumbers, their IR and Raman intensities corresponding to the different normal modes are used for identifying the vibrational modes. It can be noted that the calculated results are harmonic frequencies while the observed frequencies contain anharmonic contribution. The later is, generally, lower than the former due to anharmonicity. In fitting the calculated wavenumbers to the experimental ones, two types of scaling factors are used; dual scaling factors (0.9659 for ω_i>1700 cm^{-1}; 0.9927 for ω_i<1700 cm^{-1}) and uniform scaling factor[13] of 0.9614. For B3LYP/6-31+G (d), 6-311++G (d,p), standard deviations of 13 and 7 cm^{-1} for dual scaling method and 23 and 17 $cm^{-1,}$ respectively for uniform scaling method are obtained. Uniform scaling does an excellent job in diminishing the number of extreme outliers. But experimental vibrational spectra are usually discussed in terms of different wavenumber regions corresponding to different types of vibration. High-energy modes can be expected to be more anharmonic, leading to greater errors because of the

Table 1 — Geometric parameters of 3'-(triflouromethyl)acetophenone

Bond length (Å)	a	b	Exp.	Bond angle (°)	a	b	Exp.
C1–C2	1.401	1.401	1.395	C2–C1–C6	119.5	119.1	120.0
C1–C6	1.403	1.406	1.395	C2–C1–C7	124.7	122.3	120.0
C1–C7	1.516	1.504		C1–C2–C3	119.3	120.2	120.0
C2–C3	1.403	1.400	1.395	C1–C2–H13	120.9	120.6	120.0
C2–H13	1.082	1.085	1.100	C6–C1–C7	115.8	118.6	120.0
C3–C4	1.393	1.396	1.395	C1–C6–C5	120.8	120.5	120.0
C3–C14	1.516	1.506		C1–C6–H20	117.9	118.3	120.0
C4–C5	1.392	1.399	1.395	C1–C7–O8	119.3	120.1	120.0
C4–H18	1.080	1.085	1.100	C1–C7–C9	120.0	119.2	120.0
C5–C6	1.385	1.391	1.395	C3–C2–H13	119.8	119.1	120.0
C5–H19	1.083	1.086	1.100	C2–C3–C4	120.5	120.4	120.0
C6–H20	1.083	1.085	1.100	C2–C3–C14	121.5	118.5	120.0
C7–O8	1.217	1.223	1.208	C4–C3–C14	118.0	121.2	120.0
C7–C9	1.514	1.517	1.512	C3–C4–C5	120.1	119.5	120.0
C9–H10	1.097	1.097	1.113	C3–C4–H18	119.8	120.1	120.0
C9–H11	1.097	1.097	1.113	C3–C14–F15	111.5	112.8	
C9–H12	1.090	1.092	1.113	C3–C14–F16	112.6	111.8	
C14–F15	1.353	1.353		C3–C14–F17	112.6	111.8	
C14–F16	1.358	1.361		C5–C4–H18	120.2	120.4	120.0
C14–F17	1.358	1.361		C4–C5–C6	119.9	120.3	120.0
				C4–C5–H19	119.9	119.7	120.0
				C6–C5–H19	120.2	120.1	120.0
				C5–C6–H20	121.4	121.1	120.0
				O8–C7–C9	120.7	120.7	120.0
				C7–C9–H10	111.0	111.2	109.5
				C7–C9–H11	111.0	111.2	109.5
				C7–C9–H12	108.9	108.8	109.4
				H10–C9–H11	107.0	107.3	109.4
				H10–C9–H12	109.5	109.2	109.5
				H11–C9–H12	109.5	109.2	109.5
				F15–C14–F16	106.8	107.0	
				F15–C14–F17	106.8	107.0	
				F16–C14–F17	106.0	106.2	

a-calculated by B3LYP/6-31+G(d), b-calculated by B3LYP/6-311++G(d,p).

harmonic approximation. So "dual scaling factor procedure" was adopted. The dual scaling procedure does an excellent job in improving the error distribution between the scaled theoretical frequencies and experimental fundamental frequencies. The dual scaled error distributions for B3LYP/6-311++G(d,p) are more symmetric, compared with the uniform scaled frequency errors. Figure 4 shows the histograms which show a marked improvement using dual scaling.

4.3.1 C–H vibration

In the present study, the four hydrogen atoms, which are attached to the benzene ring of 3′-TFMA give rise to four C–H stretching modes, four C–H in-plane bending and four C–H out-of-plane bending modes. Usually, the aromatic organic molecule shows the presence of the C–H stretching vibrations in the wavenumber region 3000–3100 cm^{-1} and it is the characteristic region for the identification of C–H stretching vibrations[14]. For 3′-TFMA molecule, the aromatic C–H stretching modes are assigned to 3075, 3047 cm^{-1} in FT-IR and 3090, 3020 cm^{-1} in FT-Raman. The potential energy distribution (PED) results showed that, these modes are very pure. In aromatic compounds, the C–H in-plane and out-of-plane bending vibrations[15,16] appear in the range 1000-1300 cm^{-1} and 750-1000 cm^{-1}, respectively. FT-IR bands at 930, 1015 and 1180 cm^{-1}, its Raman counterpart at 1176 cm^{-1} are assigned to C–H in-plane bending modes. The weak bands observed at 965 cm^{-1}, 600 cm^{-1} in FT-IR, its Raman counterpart at

Table 2 — Fundamental band assignments of 3′-(triflouromethyl)acetophenone

Mode	Experimental wavenumber (cm^{-1})		Theoretical wavenumber (cm^{-1})						IR intensities		Raman intensities		Vibrational Assignments
	FT-IR	FT-Raman	Unscaled		Scaled dual scaling		Scaled uniform scaling						
			a	b	a	b	a	b	a	b	a	B	
A		3090w	3231	3209	3121	3100	3142	3121	4.734	2.661	0.959	1.292	νCH(98)
A	3075w		3226	3202	3116	3093	3138	3114	1.022	2.105	0.305	0.504	νCH(96)
A	3047w		3220	3199	3110	3090	3132	3111	1.002	0.421	0.277	0.353	νCH(97)
A		3020vw	3202	3182	3093	3073	3114	3095	6.542	4.302	0.486	0.579	νCH(98)
A	3003w		3165	3146	3057	3039	3078	3060	9.695	9.442	0.579	0.760	νCH_3asym(98)
A			3107	3092	3001	2987	3022	3007	6.913	5.938	0.266	0.353	νCH_3asym(98)
A	2900vw		3050	3034	2946	2931	2966	2951	2.751	2.226	0.872	1.331	νCH_3sym(97)
A	1702vs	1700m	1760	1754	1700	1694	1712	1706	200.21	207.65	1.582	2.035	νC=O(90)
A	1615ms	1622m	1659	1647	1647	1635	1614	1602	17.56	16.665	1.334	1.766	νCC_{aro}(81), δCH (13)
A	1597sh	1600w	1640	1628	1628	1616	1595	1583	15.88	15.514	1.169	1.532	νCC_{aro}(76),δCH(18)
A	1518w		1529	1516	1518	1505	1487	1474	4.002	3.754	0.073	0.101	νCC_{aro}(72),δCH(17)
A	1480w		1502	1479	1491	1468	1461	1438	12.992	12.236	0.303	0.353	δ CH_3 (90)
A		1470vw	1493	1471	1482	1460	1452	1431	10.867	10.935	0.218	0.250	γ CH_3(88)
A	1442ms	1450w	1468	1459	1457	1448	1428	1419	27.083	26.130	0.054	0.074	νCC_{aro}(75), δCH (12)
A	1372ms		1411	1389	1401	1379	1372	1351	48.121	56.503	0.091	0.133	δCH_3(umb)(77),δCC(21)
A	1350s	1350w	1373	1357	1363	1347	1335	1320	122.96	146.61	0.088	0.124	νCC_{aro}(65), δCH (20)
A		1280w	1348	1338	1338	1328	1311	1301	9.354	8.246	0.659	1.060	νCC_{aro}(67),δCH(19)
A			1335	1322	1325	1312	1298	1286	71.482	53.452	0.818	0.939	$\nu CC(CF_3)$(60), νCC_{aro}(17)
A	1255s		1263	1249	1254	1240	1228	1215	356.35	362.92	0.484	0.634	$\nu CC(C{=}O)$(62),νCC_{aro}(12)
A	1180w	1176w	1205	1196	1196	1187	1172	1163	6.581	8.18	0.264	0.330	δCH(75), νCC(15)
A	1133w		1169	1156	1160	1148	1137	1124	133.77	125.36	0.149	0.180	νCF(80), δCH(12)
A	1105sh		1125	1117	1117	1109	1094	1086	47.785	57.212	0.046	0.057	νCF(75), δCH(22)
A			1121	1105	1113	1097	1090	1075	7.342	10.36	0.115	0.140	δCH(66),νCC_{aro}(22),νCF(10)
A		1098vs	1107	1100	1099	1092	1077	1070	272.34	281.36	3.468	4.653	νCF(81), νCC_{aro}(15)
A	1075ms	1071vw	1082	1078	1074	1070	1052	1048	122.22	132.17	0.603	0.702	oprCH_3(69),νCF(15)
A	1033w		1054	1044	1046	1036	1025	1015	0.884	0.7287	0.019	0.020	iprCH_3 (80)
A	1015w		1017	1017	1010	1010	989	989	3.269	2.617	2.149	3.109	δCH(92)
A	965w		1016	1015	1009	1008	988	987	0.923	0.845	0.001	0.000	γCH(90)
A			967	963	960	956	941	937	1.083	0.949	0.413	0.010	δring1(75),νCC(11)
A	930m		965	958	958	951	939	932	25.053	27.203	0.009	0.567	δCH(61),νCC_{aro}(27)
A	905w		929	920	922	913	904	895	11.181	11.354	0.007	0.008	$\nu CC(CH_3)$(75)
A		825vw	835	833	829	827	812	810	8.970	8.442	0.088	0.126	γCH(68),νCC(20)
A	810s		827	826	821	820	804	803	40.156	40.258	0.011	0.011	δCC (72),νCC(16)
A		722ms	723	725	718	720	703	705	2.996	3.506	1.568	2.041	δC=O(70),δring(12)
A	698s		705	704	700	699	686	685	24.866	25.979	0.002	0.001	γ CC(65), γ CH(20)
A	665s	653w	659	662	654	657	641	644	15.439	14.865	0.025	0.494	δ ring2 (60), δCF_3(22)
A	600m	596vw	659	654	654	649	641	636	2.0356	1.588	0.320	0.066	γ CH (68),γ ring3 (21)
A	585w	580vw	604	605	600	601	587	588	29.838	29.91	0.230	0.309	δring3(66), δCC (22)
A			572	576	568	572	556	560	1.744	1.718	0.071	0.108	δCC(70),δring(21)
A			567	566	563	562	551	550	3.564	3.126	0.068	0.115	γ ring1(70), γ CH(18)
A		483vw	480	483	476	479	467	470	0.102	0.142	0.049	0.059	δCF_3(u)(84), δCC(12)
A			480	481	476	477	467	468	0.718	0.578	0.141	0.163	γ ring2(75), γ CC(15)
A		420vw	427	421	424	418	415	409	0.096	0.184	0.026	0.033	γ CC(65), γ ring(20)
A			391	393	388	390	380	382	3.788	4.047	0.523	0.684	γ CH (78), γ ring3 (10)
A		366vw	364	365	361	362	354	355	1.365	1.145	0.509	0.684	γ CF3(66),γring(11)
A			323	323	321	321	314	314	0.104	0.157	0.089	0.086	δCF_3(74), δring(12)
A		305w	312	312	310	310	303	303	2.174	2.144	1.895	2.592	iprCF_3(70),δring(22)
A			242	242	240	240	235	235	2.266	2.214	0.099	0.149	oprCF3(65),ƮCF3(20)
A		168ms	167	165	166	164	162	160	0.116	0.073	2.200	3.102	γC=O(68), γ CH(20)
A		153ms	164	155	163	154	160	151	0.104	0.073	0.060	0.136	γring3(78),γ CH(10)
A			126	126	125	125	123	123	4.159	4.224	0.399	0.547	δC-CF_3(55), δC-C=O(25)
A			117	115	116	114	114	112	0.016	0.026	5.255	7.144	τCH_3(61), γ CH(32)
A			49	45	49	45	48	44	7.145	7.009	6.495	9.417	ω$COCH_3$(75), γ ring(12)
A			16	19	16	19	16	18	0.059	0.040	100.0	100.00	τCF_3(59), γ CH(32)

ν-stretching, δ-in-plane bending, r-rocking, u-umbrella vibration (symmetric deformation), ω-wagging, τ-torsion, γ-out-of plane bending, ipr– In-plane rocking, opr-out-of-plane rocking, sh-shoulder. a-calculated by B3LYP/6-31+G(d), b-calculated by B3LYP/6-311++G(d,p).

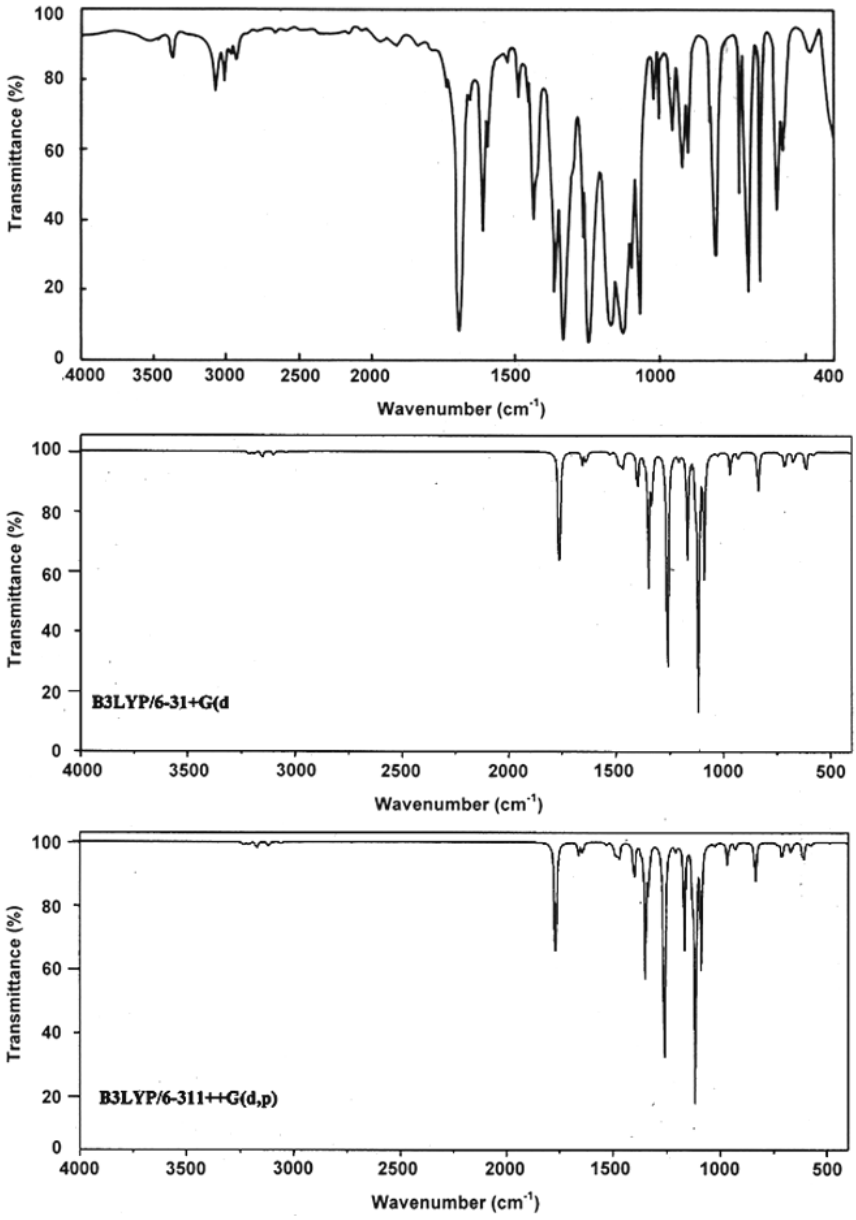

Fig. 2 — Observed and simulated IR spectra of 3′-(triflouromethyl) acetophenone

596 cm^{-1} and FT-Raman band at 825 cm^{-1} are assigned to C–H out-of plane bending modes.

4.3.2 Methyl group vibrations

The methyl substitution on the benzene ring of the title molecule consists of nine fundamental vibrational modes. The methyl stretching vibrations, generally, maintain their characteristic positions i.e. C–H stretching vibrations of the methyl group lay in the region 2840-2975 cm^{-1}. Methyl group vibrations[17-20] are, generally, referred to electron donating substituent in the aromatic ring system, the asymmetric C–H stretching mode of CH_3 is expected at 2980 cm^{-1} and the symmetric C–H stretching mode is expected at 2870 cm^{-1}. In 3′-TFMA, a weak infrared band at 3003 cm^{-1}, a weak Raman band at 2931 cm^{-1} are assigned to CH_3 asymmetric stretching vibrations. A weak IR band at 2900 cm^{-1} is assigned to CH_3 symmetric stretching vibrations. The percentage of PED shows that, the methyl C–H stretching modes are pure like aromatic C–H stretching. Generally, aromatic compound displays

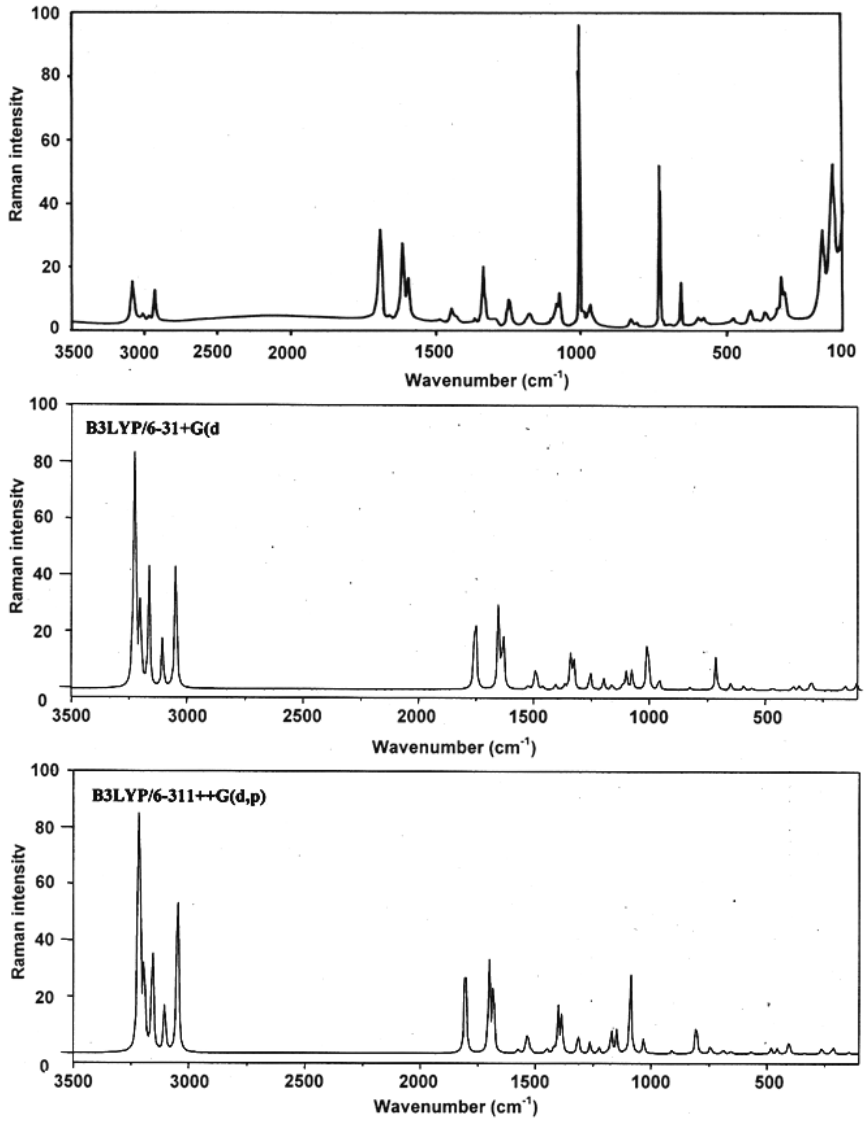

Fig. 3 — Observed and simulated Raman spectra of 3′-(triflouromethyl) acetophenone

the methyl in-plane and out-of plane rocking vibration bands in the neighbourhood of 1045 cm^{-1} and 970±70 cm^{-1}, respectively[21–23]. In the present study, the weak band at 1033 cm^{-1} in FT-IR corresponds to in-plane rocking vibration; out-of plane rocking vibration is observed as a medium strong band at 1075 cm^{-1} (FT-IR) and its very weak Raman counterpart at 1071 cm^{-1}. The calculated value of 115 cm^{-1} at B3LYP/6-311++G(d,p) method is assigned to the twisting mode of the methyl group. The CH_3 in-phase ("umbrella") deformation is strongly dependent upon the electronegativity of the adjacent atom. The more electronegative the atom, the higher will be the frequency with a range[24] of 1470–1250 cm^{-1}. The 3′-TFMA shows a medium strong symmetric umbrella deformation mode at 1372 cm^{-1} (FT-IR). The in-plane and out-of plane bending vibrations of 3′-TFMA are assigned in the characteristic region.

4.3.3 Ring vibrations

Aromatic ring vibrations occur in the region 1620-1420 cm^{-1}. Sharp bands in this region involve the aromatic ring quadrant and semi-circle stretching vibrations. The IR intensities of these bands are variable in intensity. The Raman intensities are moderate for the quadrant stretching and quite weak for the semi-circle stretching bands. The quadrant

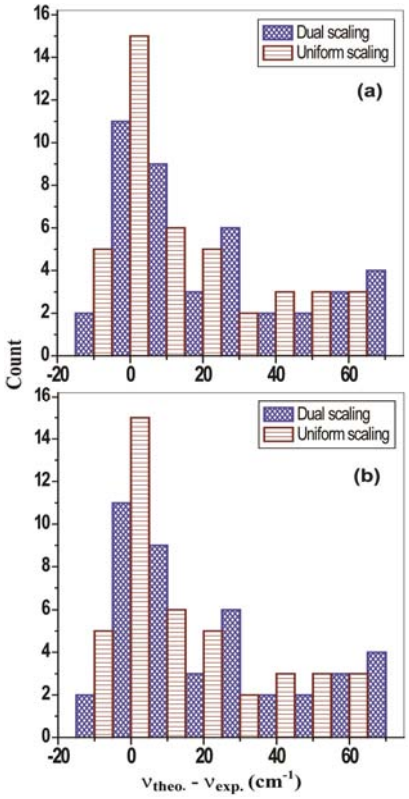

Fig. 4 — Histogram of the frequency differences between experimental and scaled frequencies by B3LYP/6-31+G(d) & 6-311++G(d,p) of 3′-(triflouromethyl) acetophenone

stretch will result in bands[24] near 1600-1580 cm^{-1} while 1578 semicircle stretch result in bands near 1500-1460 cm^{-1}. The FT-IR bands at 1615, 1597, 1518, 1442, 1350 cm^{-1} and FT-Raman bands at 1622, 1600, 1450, 1350, 1280 cm^{-1} are assigned to ring stretching vibrations. The ring in-plane and out-of-plane bending vibrations are assigned in the characteristic regions.

4.3.4 CF_3 vibrations

The bands due to the C–F stretching vibration may be found over a wide frequency range, 1360-1000 cm^{-1} since the vibration is easily influenced by adjacent atoms or groups. Due to strong coupling of the C–F and C–C stretching vibration, poly flourinated compounds have a series of very intense bands in the region 1360-1090 cm^{-1}. Aromatic flouro compounds have a band of variable intensity in the region 420-375 cm^{-1} due to in-plane deformation[25].

In the halogen atom, the C–H stretching shifts to higher wave number due to the –I effect of the halogen atom. Due to the –I effect of halogen, C–H part of the molecule becomes rich in *s*-component, and hence, force constant increases. The greater electro-negativity of the halogen atom, greater is the value of C–H stretching. C–F bonds show lower values of absorption frequencies as compared to C–H bond due to the decreased force constant and increase in the reduced mass[15]. Weaker FT-IR bands at 1133, 1105 cm^{-1} and relatively strong Raman band located at 1098 cm^{-1} are assigned to CF_3 stretching vibrations. A relatively weak FT-Raman band at 483 cm^{-1} is assigned to the symmetric CF_3 deformation vibration (umbrella vibration). The in-plane rocking vibration is assigned to a weak Raman band at 305 cm^{-1} while out-of plane bending vibration is assigned to a very weak Raman band at 366 cm^{-1}. No characteristic bands are observed for out-of-plane rocking and in-plane bending vibrations of 3′-TFMA. The calculated values at 19 cm^{-1} are assigned to twisting vibrations of the title compound.

4.3.5 C=O vibrations

Carbonyl group vibrations in ketones are the best characteristic bands in vibrational spectra, and for this reason, such bands have been the subject of extensive studies. The intensity of these bands can increase because of conjucation, therefore, leads to the intensification of the Raman lines as well as the increased infrared band intensities. The carbonyl-stretching vibrations[26,27] in ketones are expected in the region 1680–1715 cm^{-1}. In 3′-TFMA, a very strong and intense FT-IR band at 1702 cm^{-1} and medium intensity FT-Raman band at 1700 cm^{-1} are assigned to C=O stretching vibration, which lies in the expected range of ketones. A medium to strong intensity FT-Raman bands at 722 and 168 cm^{-1} are assigned to in-plane and out-of-plane C=O deformation modes.

4.4 Mulliken atomic charges

Table 3 gives the values of atomic charges of 3′-TFMA calculated by DFT method using 6-31+G(d), 6-311++G(d,p) basis set. The deactivating groups direct the reaction to meta positions[28,29]. The carbonyl carbon (C7) bears a partial positive charge due to the electron withdrawing effect of the oxygen atom. This in turn has an inductive withdrawing effect on the phenyl ring. Hence, carboxy methyl group is withdrawing group by inductive as well as resonance effects. These twin effects have directed a substitution at meta position. Since tri flouro methyl group is also a deactivating group, fluorine atoms withdraw the

Table 3 — Mulliken atomic charges of 3′-(triflouromethyl)acetophenone

Atoms	6-31+G(d)	6- 311++G(d,p)	Atoms	6-31+G(d)	6-311++G(d,p)
C1	0.745322	0.745322	H11	0.233436	0.162630
C2	0.06291	0.0785015	H12	0.246529	0.217086
C3	– 1.787185	– 1.232875	H13	0.210917	0.170577
C4	– 0.559607	– 1.107137	C14	1.570411	0.916881
C5	– 0.393851	– 0.187398	F15	– 0.334165	– 0.140204
C6	0.373771	0.337303	F16	– 0.273296	– 0.067848
C7	0.544057	0.341381	F17	– 0.27325	– 0.067713
O8	– 0.423211	– 0.234834	H18	0.216314	0.170914
C9	– 0.819654	– 0.447511	H19	0.197458	0.191320
H10	0.233447	0.162626	H20	0.229646	0.199351

electrons away from the C14 atom due to the inductive effect and hence C14 atom accommodates maximum positive charges and adjacent C3 atom is more negative. All electronegative (oxygen and fluorine) atoms carry negative charges; all electropositive hydrogen atoms carry positive charges and charge on carbon atoms can either be negative or positive depending on their positions.

4.5 HOMO–LUMO analysis

The HOMO–LUMO analysis for 3′-TFMA was carried out by B3LYP method using 6-311++G(d,p) basis set. Using HOMO and LUMO energies, quantum chemical parameters[30] were also calculated which are presented in Table 4. The frontier molecular orbital pictures are shown in Fig. 5. The orbital determines the way in which the molecule interacts with other species. HOMO is the orbital that acts as an electron donor, and LUMO is the orbital that acts as an electron deficient and hence most subject to nucleophilic attack[31,32]. In most of the cases, even in the absence of inversion symmetry, the strongest bands in the Raman spectrum are weak in the IR spectrum and vice-versa. The π electron cloud movement from the donor to acceptor can make the molecule highly polarized through the single-double bond path when it changes from the ground state to the first excited state. An electronic system with a larger HOMO–LUMO gap should be less reactive than one having smaller gap. Both the highest occupied molecular orbital (HOMO) and lowest unoccupied molecular orbital (LUMO) are the main orbital taking part in chemical stability[33,34].

A molecule with a small gap is more polarized and is known as soft molecule. In 3′-TFMA, the energy gap is small. Hence, it is thermodynamically favourable for an electron transfer to occur. Chemical potential or Fermi energy represents the change in Gibbs energy per atom. Low value of energy gap is also due to electron-withdrawing groups that enter into conjugation. Moreover, the Fermi energy lies exactly in the midst of the HOMO and LUMO in 3′-TFMA. Large values of electron affinity and electrophilicity in 3′-TFMA confirm that it prefers to accept more number of electrons. Homo orbital is most heavily concentrated on carbonyl group and methyl group, meaning that electrophilic attack will likely occur here. LUMO is over the carbonyl carbon which confirms that carbonyl compounds undergo nucleophilic addition at the carbonyl carbon. LUMO is also located over the aromatic ring.

Table 4 — HOMO–LUMO analysis and quantum chemical parameters of 3′-(triflouromethyl)acetophenone calculated by B3LYP/6-311++G(d,p)

Parameters	Quantum chemical parameters	
	In a.u.	In eV
HOMO	– 0.27541	– 7.4943366
LUMO	– 0.08666	– 2.358154
LUMO–HOMO	0.18875	5.1361895
Hardness	0.094375	2.5680913
Electronegativity	0.181035	4.9262453
Softness	10.59603	288.33444
Chemical potential	– 0.18104	– 4.9262453
Global Electrophilicity	0.173635	4.7248891

4.6 NBO analysis

In hydrogen bonded systems, the stability of the molecule may cause several factors; Hyper conjugative interactions, inter, intramolecular hydrogen bonding, intermolecular charge transfer (ICT), electron density transfer (EDT) and effect due

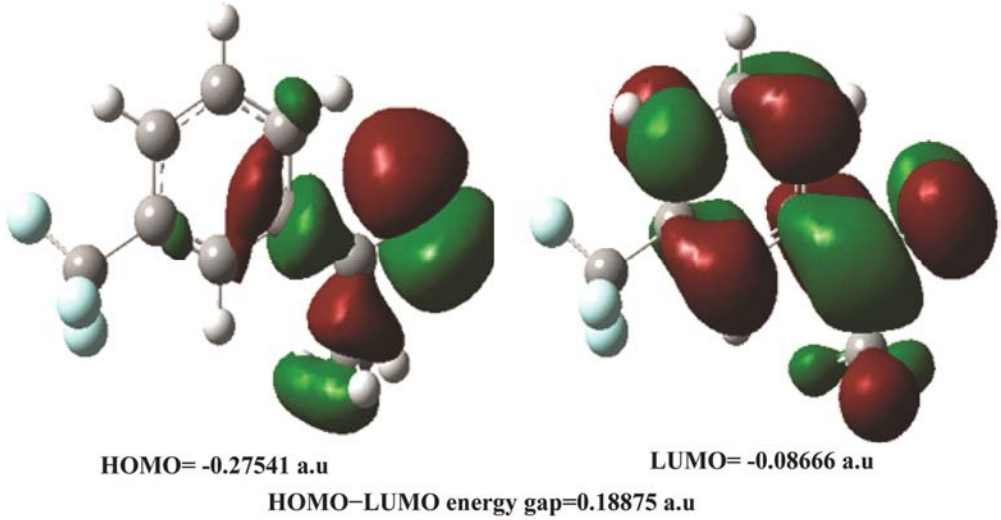

Fig. 5 — Electron density surface plots of the frontier molecular orbitals with their energies (a.u) of 3′-(triflouromethyl)acetophenone

to the delocalization of electron density from filled lone pairs into the unfilled anti-bonding of Lewis acid. Natural Bond Orbital (NBO) analysis is an effective tool for determining the above mentioned factors[35]. NBO theory allows the assignment of the hybridization of atomic lone pairs and of the atoms involved in bond orbitals. Interaction between atomic orbitals can be interpreted using NBO theory. NBO also gives the accurate natural Lewis structure picture of 3′-TFMA since it gives the maximum percentage of electron density. The second order Fock matrix was carried out to evaluate donor (*i*) and acceptor (*j*). The stabilization energy $E^{(2)}$ associated with a delocalization $i \rightarrow j$ is estimated as follows:

$$E^{(2)} = \Delta E_{ij} = q_i \frac{F_{(i,j)}^{\ 2}}{\varepsilon_j - \varepsilon_i}$$

where q_i is the donor orbital occupancy, j and I are diagonal elements and $F_{(i,j)}$ is the off-diagonal NBO Fock matrix element[36–38]. Hyper conjugation is an important effect in which an occupied Lewis-type NBO is stabilized by overlapping with a non-Lewis type orbital. This electron delocalization can be described as a charge transfer from a Lewis valence orbital with a decrease in its occupancy to a non-Lewis. Several other types of valuable data, such as hybridization, and partial charges, have been analyzed from the NBO results[39,40].

The strongest delocalisations involves the interaction of F15 and F16 lone pair with adjacent CF anti-bonds. The interactions stabilize by 12.24 kcal/mol in Table 5. Interaction between lone pair donor and anti-bonding acceptor orbital weakens the bond associated with the anti-bonding orbital. The interaction of lone pair orbital on oxygen atom (O8) with σ^* CC bond stabilizes by 11.89 kcal/mol.

Table 5 — Second-order perturbation theory analysis of Fock matrices of 3′-(triflouromethyl)acetophenone calculated by B3LYP/6-311++G(d,p).

Donor (i)	Acceptor (j)	E(2) kcal/mol	E(j)–E(i) a.u.	F(i,j) a.u.
$n_3(F_{15})$	$\sigma^*(C_{14}–F_{16})$	11.34	0.63	0.063
$n_3(F_{15})$	$\sigma^*(C_{14}–F_{17})$	12.24	0.50	0.178
$n_3(F_{16})$	$\sigma^*(C_{14}–F_{17})$	12.24	0.05	0.192
$n_3(F_{17})$	$\sigma^*(C_{14}–F_{15})$	11.34	0.45	0.195
$n_3(F_{17})$	$\sigma^*(C_{14}–F_{16})$	11.62	1.15	0.239
$n_3(F_{17})$	$\sigma^*(C_{14}–F_{15})$	14.22	1.15	0.115
$n_3(F_{17})$	$\sigma^*(C_{14}–F_{16})$	14.14	1.15	0.114
$n_2(O_8)$	$\sigma^*(C_1–C_7)$	11.89	0.61	0.024

Bond formations between the atoms due to the overlap of different hybrids and NBO occupancies at bond critical points are listed in Table 6. The NBO occupancies of C7–O8, C14–F15, C14–F16, C14–F17 bonds are larger than those of other bonds indicating that the strength of the C–O and C–F bonds are larger than those of other bonds.

Polarization in the bond means carbon is more skewed towards flourine and oxygen atoms, because flourine and oxygen atoms are more electronegative than carbon atoms. On the contrary, the π^* anti-bonding

Table 6 — Hybrid compositions of 3′-(triflouromethyl)acetophenone calculated by B3LYP/6-311++G(d,p)

BOND(A–B)	ED/ENERGY	ED_A (%)	ED_B (%)	NBO	S (%)	P (%)
BD(1)C1–C6	1.97121	50.31	49.69	0.7093 ($SP^{1.84}$)+0.7049($sp^{1.75}$)	35.19 36.39	64.81 63.61
BD*(1)C1–C6	0.02402	49.69	50.31	0.7049 ($SP^{1.84}$)– 0.7093 ($sp^{1.75}$)	35.19 36.39	64.81 63.61
BD(2)C1–C6	1.59335	54.92	45.08	0.7411(P)+0.6714(P)	00.00 00.00	100.00 100.00
BD*(2)C1–C6	0.35611	45.08	54.92	0.6714 (P)– 0.7411 (P)	00.00 00.00	100.00 100.00
BD(1)C1–C7	1.97869	52.60	47.40	0.7253($SP^{2.40}$)+0.6884($SP^{1.78}$)	29.37 36.00	70.63 64.00
BD*(1)C1–C7	0.05337	47.40	52.60	0.6884 ($SP^{2.40}$)– 0.7253 ($SP^{1.78}$)	29.37 36.00	70.63 64.00
BD(1)C2–C3	1.97260	49.49	50.51	0.7035($SP^{1.78}$)+0.7107($SP^{1.74}$)	35.96 36.45	64.04 63.55
BD*(1)C2–C3	0.02307	50.51	49.49	0.7107 ($SP^{1.78}$)– 0.7035 ($SP^{1.74}$)	35.96 36.45	64.04 63.55
BD(2)C2–C3	1.66508	45.86	54.14	0.6772(P)+0.7358(P)	00.00 00.00	100.00 100.00
BD*(2)C2–C3	0.35352	54.14	45.86	0.7358 (P)– 0.6772 (P)	00.00 00.00	100.00 100.00
BD(1)C2–H13	1.97732	61.42	38.58	0.7837($SP^{2.61}$)+0.6211(S)	27.68 100	72.32 00.00
BD*(1)C2–H13	0.01530	38.58	61.42	0.6211($SP^{2.61}$)– 0.7837 (S)	27.68 100	72.32 00.00
BD(1)C7–O8	1.99272	36.55	63.45	0.6046($SP^{2.55}$)+0.7966($SP^{3.18}$)	28.13 23.92	71.87 76.08
BD*(1)C7–O8	0.01669	63.45	36.55	0.8091 ($SP^{2.55}$)– 0.5877 ($SP^{3.18}$)	28.13 23.92	71.87 76.08
BD(1)C3–C14	1.98464	50.15	49.85	0.7082($SP^{2.70}$)+0.7060($SP^{1.89}$)	27.01 34.60	72.99 65.40
BD*(1) C3–C14	0.06305	49.85	50.15	0.7060 ($SP^{2.70}$)– 0.7082 ($SP^{1.89}$)	27.01 34.60	72.99 65.40
BD(1)C14–F15	1.99467	28.11	71.89	0.5302($SP^{3.60}$)+0.8479($SP^{3.08}$)	21.76 24.50	78.24 75.50
BD*(1)C14–F15	0.10019	71.89	28.11	0.8479 ($SP^{3.60}$)–0.5302 ($SP^{3.08}$)	21.76 24.50	78.24 75.50
BD(1)C14–F16	1.99467	28.11	71.89	0.5302($SP^{3.60}$)+0.8479($SP^{3.08}$)	21.76 24.50	78.24 75.50
BD*(1)C14–F16	0.10019	71.89	28.11	0.8479 ($SP^{3.60}$)– 0.5302 ($SP^{3.08}$)	21.76 24.50	78.24 75.50
BD(1)C14–F17	1.99543	27.98	72.02	0.5289($SP^{3.61}$)+0.8487($SP^{3.03}$)	21.69 24.81	78.31 75.19
BD*(1)C14–F17	0.09212	72.02	27.98	0.8487 ($SP^{3.61}$)–0.5289 ($SP^{3.03}$)	21.69 24.81	78.31 75.19
BD(1)C9–H10	1.96910	60.80	39.20	0.7798($SP^{3.20}$)+0.6261(S)	23.79 100	76.21 00.00
BD*(1)C9–H10	0.00680	39.20	60.80	0.6261($SP^{3.20}$)– 0.7798 (S)	23.79 100	76.21 00.00
BD(1)C9–H11	1.98649	61.88	38.12	0.7866($SP^{3.06}$)+0.6174(S)	24.64 100	75.36 00.00
BD*(1)C9–H11	0.00480	38.12	61.88	0.6174 ($SP^{3.06}$)– 0.7866 (S)	24.64 100	75.36 00.00
BD(1)C–H12	1.96910	60.80	39.20	0.7798($SP^{3.20}$)+0.6261(S)	23.79 100	76.21 00.00
BD*(1)C9–H12	0.00680	39.20	60.80	0.6261($SP^{3.20}$)– 0.7798 (S)	23.79 100	76.21 00.00

orbital is skewed in the opposite direction, with a larger polarization co-efficient on the carbon atom. Hence, C–F bond is more polar than C–O bond and C–H bond is more polar than C–C bond.

4.7 Magnetic properties

Magnetic susceptibility results from the response of electronic orbits and/or unpaired spins to an applied field. In paramagnetic materials χ is positive-that is, for which M is parallel to B. The susceptibility is, however, also very small: 10^{-4} to 10^{-5}. The fact that these compounds have incomplete atomic shells: what is responsible for their paramagnetic behaviour. They all have a critical temperature below which the variation of susceptibility with temperature is very different from its variation above this temperature. A paramagnetic compound will have some electrons with unpaired spins. Paramagnetism derives from the spin and orbital angular moment of electrons. This type of magnetism occurs only in compounds containing unpaired electrons, as the spin and orbital angular momenta is cancelled out when the electrons exist in pairs. A plot of $1/\chi_m$ versus temperature is known as a Curie plot. Ideally, it should be linear if the Curie-Weiss law is obeyed. From such a plot, we can then extract the Curie constant from the inverse of the slope and the Weiss constant from the *x*-intercept[41,42]. For 3′-TFMB, Table 7 presents the variation of susceptibility with temperature and Fig. 6 shows the Curie plot. The plot shows that 3′-TFMB is paramagnetic in nature. The following linear equation (regression equation) is considered to be the best fit to predict the value of Curie constant.

y=4447x+8E–05 (R^2=1)
Curie constant=0.000225
Weiss constant=1.79897E–08

The Weiss constant is almost zero. Hence, the plot passes through the origin which proves the paramagnetic nature of 3′-TFMB.

4.8 Thermodynamic function analysis

The thermodynamic parameters of 3′-TFMA are determined from spectroscopic data by statistical

Table 7 — Magnetic properties of 3′-(triflouromethyl)acetophenone calculated by B3LYP/6-311++G (d, p)

Temp	$1/\chi_m$
50	222353.16
100	444706.32
150	667059.49
200	889412.65
250	1111765.81
300	1334118.98
350	1556472.14
400	1778825.31
450	2001178.47
500	2223531.63

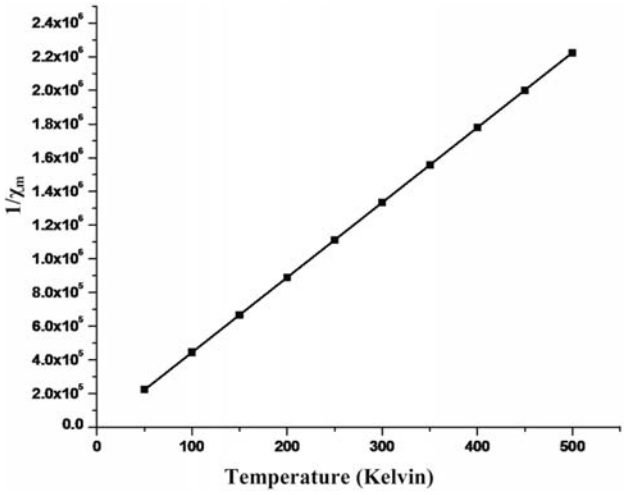

Fig. 6 — Curie plot of 3′-(triflouromethyl)acetophenone

Table 8 — Thermodynamic functions of 3'-(triflouromethyl)acetophenone calculated by B3LYP/6-311++G(d,p)

	C_P (cal/mol–Kelvin)	$(H_0 - E_0^0 / T)$ (cal/mol–Kelvin)	$(G_0 - E_0^0) / T$ (cal/mol–Kelvin)	S (cal/mol–Kelvin)
100	20.24	15.45	–65.85	81.31
200	32.49	28.25	–77.52	105.75
300	44.77	42.92	–80.88	123.81
400	56.11	58.87	–89.59	148.47
500	65.65	75.78	–92.11	167.89
600	72.46	95.17	–100.30	195.48
700	79.12	111.68	–102.78	214.46
800	84.00	130.45	–110.57	241.02
900	88.01	149.65	–113.01	262.66
1000	91.34	169.20	–116.84	276.05

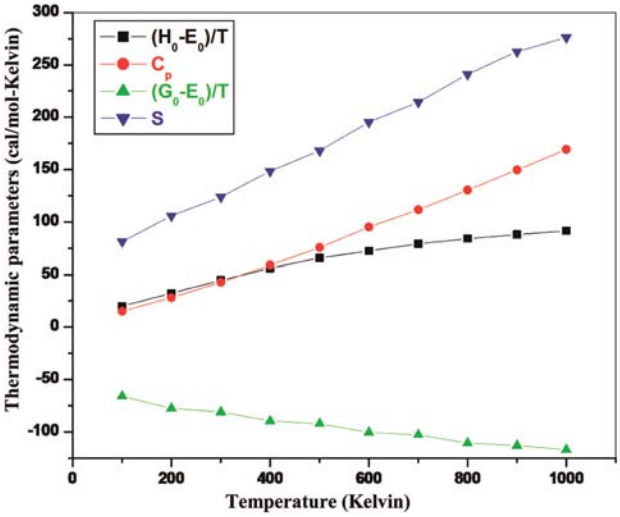

Fig. 7 — Thermodynamic plot of 3′-(triflouromethyl)acetophenone

methods[43,44]. The thermodynamic quantities such as entropy S, heat capacity (C_p), $(H^o - E^o_o)/T$ and $(G^o - E^o_o)/T$ for various temperatures are determined using the vibrational wave numbers. For numerical calculation, x_i is expressed as $x_i = hcw_i/kT = 1.439w_i/T$ where w_i is the wave number in cm^{-1}. The thermodynamic functions are calculated for the temperature range 100-1000 K and these results are presented in Table 8. The variation of thermodynamic parameters with temperature is shown in Fig. 7. The thermodynamic parameters are greater for 3′-TFMA since they depend on mass, moment of inertia and vibrational frequencies.

5 Conclusions

The optimized structure, IR and Raman intensities of the fundamental bands of 3′-TFMA were calculated using the DFT (B3LYP) methods using BLYP/6-31+G(d) and BLYP/6-311++G (d,p) basis sets. DFT method with 6-311++G(d,p) basis set yields a good description of the vibrational modes of 3′-TFMA. The good match between the experimental and calculated wavenumbers of the normal modes of 3′-TFMA molecule allows us to safely assign the vibrational spectrum of the molecule. In the fitting of the calculated harmonic wavenumbers to the corresponding experimental wavenumbers, two different scaling procedures, called 'dual scale factors' and 'uniform scaling methodology', were applied independently. Both procedures yielded results,generally, in good agreement with the experiment; however, the dual scaling methodology proved its superiority over the other. HOMO-LUMO energy gap conforms that 3′-TFMA is a soft molecule. NBO reflects the charge transfer within the molecule and it also confirms the aromatic nature of the phenyl ring of 3′-TFMA.Finally, the atomic charges, thermodynamic properties have also been studied. The magnetic susceptibility calculation confirms the existence of paramagnetism in 3′-TFMA.

References

1 Yadav R A & Singh Proc I S, *Indian Acad Sci* (*Chem Sci*) 95 (1985) 471.
2 Sittig M & Marshall, *Pharm Manufactu Encyclopedia*, Noyes publications, Jew Jersy, U.S.A, (1998).
3 Gadamasetti K & Tamim B, *Pro Chem in the Pharmac Industry,* CRC Press, (2007).
4 Burdock & George A, *Fenaroli's Handbook of Flavor Ingredients* (5th ed), CRC Press, (2005).
5 Norman Conolly, *J of Mental Sci*, 32 (1887) 519.
6 Frisch M J, Trucks G W & Schlegal H B, *Gaussian*, Inc, Wallingford CT, (2009).
7 Frisch A, Nielsen A B & Holder A J, *Gauss View Users Manual*, Gaussian Inc, (2008).
8 Sundius T, *MOLVIB*, 807 (1991).
9 Keresztury G, Holly S, Varga J, Besenyei G, Wang A Y & Durig J R, *Spectrochim Acta*, 49 (1993) 2007.
10 Keresztury G, Chalmers J M & Griffith P R, *Raman Spectroscopy*, John Wiley & Sons Ltd, 1 (2002).
11 Polavarapu P L, *J Phys Chem*, 94 (1990) 8106.
12 Udhayakala P, Rajendiran T V, Seshadri S & Gunasekaran S, *J Chem Pharm Res,* 3 (2011) 610.
13 Mathew D Halls, Julia Velkovski & Bernhard Schlegel H, Theor *Chem Acc,* 105 (2001) 413.
14 Kalsi P S, *Spectroscopy of Organic Compounds*, New Age International Publishers, Wiley Eastern Limited, 1993.
15 Sharma Y R, *Elementary Organic Spectrosc,* S Chand & Company Limited, (2007).
16 Colthup N B, Daly L H & Wiberley S E, Introduction to Infrared and Raman Spectroscopy, Academic Press, New York, 1990.
17 Sajan D, Hubert Joe I & Jayakumar V S, *J Raman Spectrosc*,37 (2005) 508.
18 Dollish F R, Fateley W G & Bentley F F, Characteristic Raman Frequencies of Organic Compounds, Wiley, New York, 1997.
19 Roeges N P G, A Guide to the Complete Interpretation of Infrared Spectra of Organic Structures, Wiley, New York, 1994.
20 Arivazhagan M, Krishnakumar V, John Xavier R, Ilango G & Balachandran V, *Spectrochim Acta*, 72 (2009) 94.
21 Krishnakumar V & Mathamal R, *J Raman Spectrosc*, 40 (2009) 264.
22 Lin-vien D, Cothup N B, Fateley W G & Graselli J G, The Handbook of Infrared and Raman Charecteristic Frequencies of Organic Molecules, Academic Press, Boston, (1991).
23 Diem M, Introduction to Modern Vibrational Spectroscopy, Wiley, New York, (1993).
24 Larkins P, *IR & Raman Spectros*, Principles and Spectral interpretation, Elsevier Publications, (2011).

25 Socrates G, Infrared & Raman Characteristic Group Frequencies, John Wiley and sons Ltd, England, (2001).
26 Kleinman D A, *Phys Rev*, 126 (1962) 1977.
27 Smith B, *Infrared Spectral Interpretation*, A Systematic Approach, CRC Press, Washington, DC, (1999).
28 Schore N E, & Vollhardt P C, *Organic Chemistry, New* York, W H Freeman and Company, (2007).
29 Fryhle C B & Solomons G, *Organic Chemistry,* Danvers, MA, Wiley, (2008).
30 Parr R G, Szentpaly L & Liu S, *J Am Chem Soc,* 12 (1999) 1922.
31 Uesugi Y, Mizuno M, Shimojima A & Takahashi H, *J Phys Chem*, 101 (1997) 268.
32 Pearson R G, *Proc Natl Acad Sci*, 83 (1986) 8440.
33 Atalay Y, Avci D & Soglu A B A, *Struct Chem,* 19 (2008) 239.
34 Vijayakumar T, Hubert Joe I, Nair C P R & Jayakumar V S, *Chem Phys,* 343 (2008) 83.
35 Politzer P & Lane P, *Struct Chem*, 1 (1990) 159.
36 Ricardo A E Castrob, Joao Canotilhob, Sandra C C Nuneas, M Ermelinda, S Eusebioa & J Simoes Redinha, *Spectrochim Acta* 72 (2009) 819.
37 Szafran M, Komasa A & Adamska E B, *J Mol Struct,* (*Theochem*), 827 (2007) 101.
38 James C, Amal Raj A, Reghunathan R, Hubert Joe I & Jayakumar V S, *J Raman Spectrosc,* 37 (2006) 1381.
39 Weinhold F, *Nature*, 411(2001) 539.
40 Weinhold F & Landis C, *Valency & Bonding*, A Natural Bond Orbit Donor-Acceptor perspective, Cambridge University Press, Cambridge, (2005).
41 Van Vleck J H, The Theory of Electric and Magnetic Susceptibilities, Oxford University Press, Oxford, (1932).
42 Mool Chand Gupta, *Atomic & Molecular Spectroscopy*, New Age International Publishers, New Delhi, (2007).
43 Randhawa H S, *Modern Molecular Spectroscopy*, Macmillan India Limited, (2003).
44 Bevan Ott J & Boerio-Goates J, *Calculations from Statistical Thermodynamics*, Academic Press, (2000).